Frontiers of Environmental Science & Engineering
2025, 19(5): 63 https://doi.org/10.1007/s11783-025-1983-x

RESEARCH ARTICLE

Real-world identification of high-emitting vehicles based on near-road sensor measurement

Bo Li[1], Dongbin Wang ✉ [1], Qiang Zhang[1], Leqi Shi[1], Mingliang Fu[2], Hang Yin[2], Jingkun Jiang ✉ [1]

1. State Key Joint Laboratory of Environment Simulation and Pollution Control, School of Environment, Tsinghua University, Beijing 100084, China
2. Vehicle Emission Control Center, Chinese Research Academy of Environmental Sciences, Beijing 100012, China

HIGHLIGHTS

- Real-world high emitters were identified using roadside measurements.
- 12.6%–16.5% of total vehicles were identified as high-emitters in field campaign.
- A correct identification rate of 95% was achieved and proven via on-site inspection.

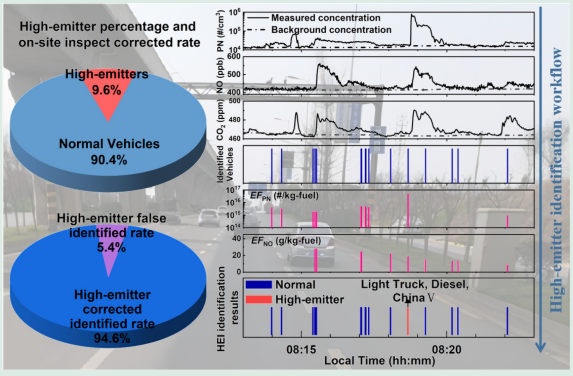

ABSTRACT: A small fraction of high-emitting vehicles make disproportionally large contributions to total fleet emissions. Therefore identifying high emitters under real driving conditions is crucial. In this study, two portable sensor platforms for high-emitter identification were used for online roadside measurements of vehicle-emitted NO, particle number (PN), and CO_2 concentrations in Tangshan and Chengdu, respectively. The measured mean concentrations of vehicle-emitted NO, PN, and CO_2 in Tangshan and Chengdu were 27.7–32.9 ppb, 5.4×10^3–8.2×10^3 #/cm^3, and 7.3–8.2 ppm, respectively. Based on more than one month of second-by-second measured pollutant concentrations and passed vehicle information, a scheme was developed to identify high emitters. Among the 217000 and 43000 vehicles that passed the roadside sensor platforms at Tangshan and Chengdu, approximately 60% and 73% of vehicle exhaust plumes were successfully detected using the sensor platform. The NO and PN emission factors (EFs) tended to have log-normal distributions with the median values of 14.3 g/kg-fuel and 1.3×10^{15} #/kg-fuel, respectively. In general, the percentages of high-emitters identified at the Tangshan and Chengdu sites were 8.7% and 12.2% of the total identified vehicles, respectively. Among these high-emitters, 122 vehicles were randomly inspected on-site with the assistance of traffic officers, and the rate of correct identification was approximately 95%, which demonstrates that our methodology performs well in identifying real-world high-emitters. Overall, its low cost, good mobility, strong adaptability, and high correct identification rate make this roadside sensor platform a promising approach for real-world high-emitter identification.

✉ Corresponding authors. E-mails: wdb2016@tsinghua.edu.cn (D. Wang); jiangjk@tsinghua.edu.cn (J. Jiang)
Article history: Received 4 November 2024, Revised 24 February 2025, Accepted 24 February 2025, Available online 15 March 2025

KEYWORDS: Real world, High-emitter identification, Roadside sensor measurement, Nitrogen oxide, Particle number

1 Introduction

Vehicle emissions have become a the major contributor to air pollutants such as nitrogen oxides (NO_x), hydrocarbons (HC), carbon monoxide (CO), and fine particulate matter (PM) in urban cities (Raparthi and Phuleria, 2022; Yang et al., 2022), which pose significant risks to air quality, public health, and climate change globally (Lelieveld et al., 2015; Anenberg et al., 2017; Carter et al., 2022; Blanco et al., 2023; Camilleri et al., 2023; Zeng et al., 2024). Despite the continuous increase in the number of new-energy vehicles, traditional fuel motor vehicles, that operate on diesel or gasoline remain the main source (Liu et al., 2021; Su et al., 2023). Vehicle emissions sources contributed approximately 31% of NO_x emissions globally and more than 45% of $PM_{2.5}$ in China's megacities (Deng et al., 2020). Several countries and regions have established strict emission standards to reduce emissions from motor vehicles. However, owing to the lack of maintenance, overload, and failure of exhaust after-treatment systems, the emissions from a small fraction of vehicles (high-emitters) in the real world can be orders of magnitude higher than the regulatory limit thresholds (Liu and Zimmerman, 2021; Chu et al., 2022; Qiu and Borken-Kleefeld, 2022; Raparthi et al., 2023). Previous studies have pointed out that 10% of high-emitters could contribute 65% PM, 40%–70% PN, and 20%–44% NO_x to total fleet emissions, respectively (Huang et al., 2018; Liu et al., 2019; Zhou et al., 2020; Liu and Zimmerman, 2021). Therefore, the identification of high-emission vehicles in the real world is important for controlling vehicle emissions.

The emission factor (EF) is a typical indicator of high-emitter identification (Huang et al., 2022). There are several approaches for determining EF from vehicle emission including cycles or bench test methods (Zheng et al., 2014; Arvind et al., 2015; Hu et al., 2021; Lei et al., 2021), portable emissions measurement systems (PEMS) (Liu et al., 2009; Kwon et al., 2017; Bishop et al., 2019), plume-chasing (Wen et al., 2019; Tong et al., 2022; Xiang et al., 2023), remote sensing (Huang et al., 2020; Heerah et al., 2021; Bishop et al., 2022; Huang et al., 2022; Qiu and Borken-Kleefeld, 2022), and stationary roadside sensor measurement (Wang et al., 2018; Raparthi and Phuleria, 2021; Shen et al., 2022). Cycle or bench tests are the primary methods for obtaining the EF. However, these test methods are conducted under controlled driving conditions, which normally underestimate the real-world emissions of individual vehicles (Chen et al., 2022). On-board PEMS and plume-chasing measurements are considered "standard methods" for obtaining real-world individual vehicle EFs. However, these approaches usually sample a limited number of individual vehicles, and the time and labor costs are high (Xiang et al., 2023), which restricts their application in routine high-emitter screening in the real world. In contrast, remote sensing and roadside sensor approaches are stationary measurements that automatically sample of fuel-specific emission factors from a large number of vehicles without interrupting traffic (Yang et al., 2022). This advantage makes remote sensing a widely used approach for monitoring individual and/or fleet vehicle emission rates (Deng et al., 2020; Bishop et al., 2022) and identifying potentially high-emission vehicles (Huang et al., 2022; Qiu and Borken-Kleefeld, 2022; Yang et al., 2022; Ghaffarpasand et al., 2023). Normally, remote sensing is based on optical principles for measuring gaseous pollutants emitted by vehicle exhaust and indirectly evaluating PM emissions according to exhaust smoke opacity to a certain extent (Feng et al., 2022). Huang et al. (2022) employed vertical remote sensing technology to detect significant percentages of in-use petrol and liquefied petroleum gas vehicles that failed to meet NO emission standards. With increasing awareness of the health impact of ultrafine particles, non-volatile particle number (PN) above 23 nm emission was regulated by the Euro-5 standard in Europe and China-6 standard in China (Wang et al., 2017; Olin et al., 2023). Particle size down to 10 nm for PN will be counted and regulated under Euro-7 (Bancă et al., 2024). Boveroux et al. (2019) demonstrated that the PN is a more useful high-emitter indicator than the exhaust smoke opacity. Compared to remote sensing methods, roadside measurements (referred to as point sampling) are cost-effective, more flexible, and not limited to gaseous pollutants (Shen et al., 2022). These advantages make roadside measurements more suitable for widespread deployment and establishment of mass-scale measurement networks.

Low-cost sensors or instruments such as $PM_{2.5}$, NO_x, sulfur dioxide (SO_2), and carbon dioxide (CO_2) analyzers are widely used to measure air quality (Apte

et al., 2017; Qiao et al., 2021; Russell et al., 2022; Bousiotis et al., 2023). To determine vehicle emission factors, roadside sensors must have reasonable accuracy and respond rapidly to highly dynamic vehicle exhaust plumes. Several studies have attempted to apply roadside sensor measurements to evaluate vehicle emissions (Wang et al., 2017; Liu et al., 2019; Chu et al., 2022; Raparthi and Phuleria, 2022; Shen et al., 2022; Raparthi et al., 2023). Wang et al. (2017) measured the mean fleet EFs of NO_x, PN, black carbon (BC), and organic aerosols on a four-lane major arterial roadway at a field measurement facility in downtown Toronto, Canada using a roadside approach. Liu et al. (2019) measured 234 city buses exhaust EFs for gaseous pollutants (NO_x, CO, and SO_2) and particles (PN and PM) under stop-and-go traffic conditions at a bus stop in Gothenburg, Sweden. Chu et al. (2022) conducted roadside measurements to determine NO_x and CO EFs using high-time-resolution sensors on a typical street canyon in Causeway Bay, Hong Kong, China. Raparthi and Phuleria (2022) and Raparthi et al. (2023) selected a semi-confined two-way canyon road and road tunnel to develop the fleet mean and individual vehicle EFs in India. In our previous study, we conducted a field experiment to investigate the viability of a compact roadside sensor platform for high-emitter identification (Shen et al., 2022). The results demonstrate that the roadside sensor platform has potential applications in successfully identifying high emitters by combining the EFs of PN and NO (Shen et al., 2022). Similarly, these studies used roadside sensors to evaluate individual and fleet vehicle emission factors in restricted driving tracks such as experimental fields and street canyons with small traffic flows and low vehicle speeds (below 20 km/h). However, high-emitter identification for real-world urban roads has rarely been reported.

In contrast to the restricted driving track scenario, real-world urban roads are characterized by high traffic volumes, high vehicle speeds, and short vehicle intervals. As vehicle exhaust plumes need to reach the roadside after vehicles pass, pollutant concentrations usually spike rapidly over a period of seconds to minutes. As a significant number of spike signals are observed in roadside measurements, identifying the corresponding vehicle emissions from these spike signals is a crucial step in the identification of high-emission vehicles. In addition, the roadside monitoring results are a superposition of the local background and vehicle emissions. To identify on-road vehicle emissions, the background level must be subtracted from the measured concentrations. Several methods have been proposed to subtract background contributions, such as the lowest percentile from a certain time window (Wang et al., 2018; Hilker et al., 2019) and the time-frequency method (Wei et al., 2021). Although the aforementioned methods are effective in separating local and background contributions, their applicability in real-world roadside measurement scenarios is unclear. Moreover, higher emitter thresholds are key factors for successfully identifying high emitters. Several methods can be used to define the high-emitter threshold, such as setting the top few percentages of emission factors (Wang et al., 2015), setting thresholds according to emission standards (Qiu and Borken-Kleefeld, 2022), and outlier methods (Raparthi et al., 2023). However, rigorous assessments of the uncertainty and effectiveness of high-emitter thresholds for identifying high-emission vehicles on real-world roads through roadside measurements are lacking. Therefore, effectively separating the background value, accurately identifying the measured vehicle-emitted pollutant concentration peaks of the corresponding vehicles, and setting up reasonable high-emission thresholds are key issues in the real-world identification of high emitters.

In this study, a near-road high-emission identification (HEI) platform consisting of a portable non-dispersive infrared (NDIR) gas analyzer, an electrochemical NO sensor, and a newly developed low-cost and compact condensation particle counter (CPC) was used for more than one month of online roadside measurement of vehicle-emitted NO, PN, and CO_2 concentrations on typical urban roads in Tangshan and Chengdu, China. Based on the HEI measurement data sets in Chengdu and Tangshan, a novel comprehensive scheme including background subtraction, individual vehicle emission identification, and high-emitter threshold setting was developed for real-world high-emitter identification. This high-emitter identification scheme was then tested by an on-site inspection of the vehicle exhaust after-treatment system with the assistance of the traffic police. Moreover, the potential implications and limitations of near-road HEI platforms are discussed.

2 Methodology

2.1 Roadside measurement sensors

In this study, we developed an HEI platform for the measurement of pollutant concentrations emitted from vehicle exhaust including NO, CO_2, and PN. These HEI platforms were set on two roadsides in typical urban areas in Tangshan and Chengdu, China. The road conditions and measurement instruments used at the

Tangshan and Chengdu sampling sites are shown in Figs. 1(a)–1(c) and the HEI structure is shown in Fig. 1(d). Specifically, a nondispersive infrared (NDIR) gas analyzer (Li-820, LI-COR, USA) was employed to quantify the CO_2 concentration. The time required for the CO_2 analyzer to reach a 90% response (t_{90}) was approximately 3 s. An electrochemical sensor (NO-B4, ALPHASENSE, UK) was used to measure NO concentration. The load resistance of the NO sensor was modified from 47 to 3.3 Ω, resulting in a reduction in the t_{90} time from approximately 30 to 5 s (Shen et al., 2022).

In addition, a low-cost and compact CPC suitable for roadside measurements was developed to measure the PN concentrations. The cost of the newly developed CPC is approximately 1000 USD, which is relatively low compared with those of the commercial CPC. This compact structure causes the HEI platform to have lower power consumption and maintenance costs. More detailed information on the developed CPC can be found in the Supporting Information (Text S1 and Fig. S1) and a previous study (Li et al., 2024). Briefly, butanol (ACS, ⩾ 99.4%, Shanghai Aladdin biochemical technology Co., Ltd., China) was used as the working fluid for the developed CPC, and the bottom cutoff particle size was 10 nm. The performance of the developed CPC was evaluated through the comparative analysis with CPC TSI-3772, USA. As shown in Fig. S1, there is a good agreement between the developed CPC and the CPC TSI-3772 with the slope and R^2 values of 1.03 and 0.999, respectively. Owing to its low cost and compact size, this newly developed CPC has great potential for mass-networked deployment. To the best of our knowledge, roadside PN concentrations generally range from 10^4 #/cm^3 to 5 × 10^6 #/cm^3, whereas the upper limit of a general CPC is approximately 10^5 #/cm^3. A customized aerosol flow diluter (DIL-001, Beijing NaKe Environmental Technologies Co., Ltd., China) with a fixed dilution ratio of 30:1 was used in this study, and the measurement range of the developed CPC can be extended to 6 × 10^6 #/cm^3. A 2-D ultrasonic anemometer (WindSonic, Gill Instruments Ltd., UK) was used to observe the wind speed and wind direction. The measurement time resolutions of the sensors is 1 Hz. The t_{90} response time of the CPC is approximately 3 s. The fast response times (approximately 3–5 s) of the NO, CO_2, and CPC sensors in this study render the HEI platform particularly well-suited for the identification of high emitters in real-world scenarios.

2.2 Sampling and data set details

Real-time measurements of vehicle exhaust emission pollutants (NO, CO_2, and PN) and vehicle information were conducted on the roadsides of Dazhao Road in

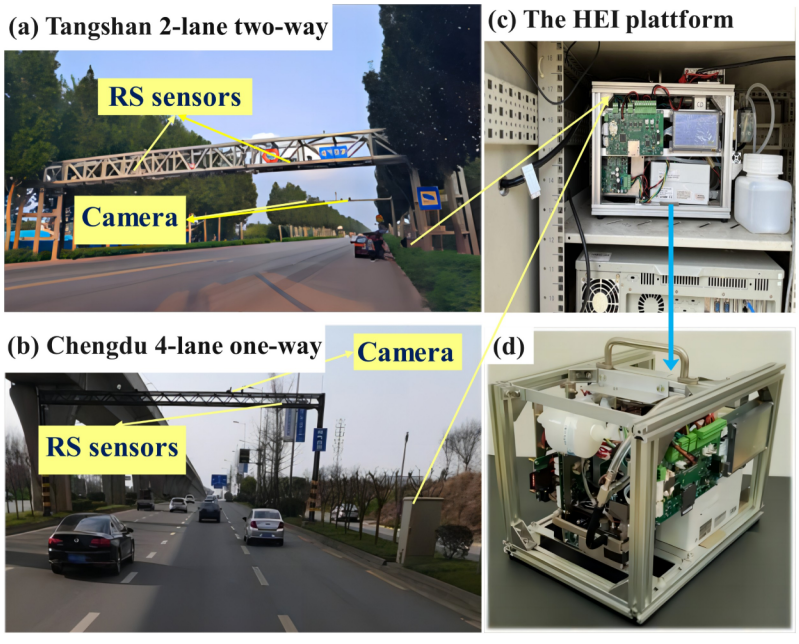

Fig. 1 Road condition and measurement instruments of the Tangshan (a) and Chengdu (b) sampling sites, (c) the HEI in the instrument shelter box, and (d) the HEI structure. Note: Cameras are used to recognize the vehicle license plate, vehicle speed, and acceleration, and RS sensors are top-down remote sensing systems.

Laoting, Tangshan (Fig. 1(a)) and Taodu Road in Chengdu (Fig. 1(b)), China. Dazhao Road is a typical 2-lane two-way road without a divider. Taodu Road in Chengdu is a 4-lane one-way road without dividers, above which road is a high-speed railway channel. The HEI platform was in an instrument shelter box and placed on one side of the road (Fig. 1(c)), and the inlet was placed outboard of the shelter box (approximately 1.2 m above ground), which was close to the height of the vehicle tailpipe. A cyclone separator for aerosol sampling was used to remove the larger particular matter (particle size larger than 2.5 μm). A top-down remote-sensing system was placed at the same site (Figs. 1(a) and 1(b)). The measurement of the remote sensing system was performed simultaneously with the HEI measurements. In this study, remote-sensing high-emitter identification results were compared with those of the HEI. In addition, vehicle speed and acceleration sensors were used to record the instantaneous speed and acceleration of the passing vehicle. A vehicle license plate recognition camera was employed to record the vehicle's passing time and number plate so that vehicle characteristics, such as vehicle emission standards, vehicle type, and fuel type, could be retrieved from the national vehicle registration databases. Additional information on the top-down remote sensing systems can be found in previous studies (Yang et al., 2022; Ghaffarpasand et al., 2023). The measurement data from the different measurement devices were processed by time synchronization.

The sampling periods for Tangshan and Chengdu were August 8th to October 20th, 2022, and April 13th to May 30th, 2023, respectively. The characteristics of the vehicle types, vehicle speed, wind speed, and wind direction during the sampling period are shown in Fig. S2. Generally, gasoline passenger cars were the dominant vehicle model, which accounted for 65.9% and 88.9% in Tangshan and Chengdu, respectively. Heavy-duty diesel trucks accounted for 11.8% in Tangshan, which was approximately 2 times higher than that in Chengdu. Similar vehicle speed distribution characteristics were observed in Tangshan and Chengdu. Both followed the fitted normal distributions, and most vehicle speeds were in ranges of 30–65 and 40–70 km/h at the Tangshan and Chengdu sites, respectively.

In addition, the track experiment data sets published in our previous study were used to determine the background subtraction method and different instrument response times to vehicle exhaust-emitted pollutants. Detailed information regarding the track experiment can be found in our previous study (Shen et al., 2022).

2.3 The high emitter identified algorithm

A workflow scheme for high-emitter identification based on long-term HEI measurements in Tangshan and Chengdu, China, is presented in Fig. S3. The measured concentrations of NO, PN, and CO_2 were processed using background subtraction. In general, the time series of pollutant concentrations ($C_{(p,i)}$) of NO, PN, and CO_2 measured by the near-road HEI platform were determined by the superposition of on-road vehicle emission source ($C_{V(p,i)}$) and local background sources ($C_{Bg(p,i)}$) for pollutant p at time i, which can be presented as follows Eq. (1).

$$C_{(p,i)} = C_{V(p,i)} + C_{Bg(p,i)}. \quad (1)$$

In this study, the specified lowest percentile from a certain time window was used to extract background concentrations from the near-road measurements. The reliability and accuracy of this method were evaluated by comparing the emission factors measured by roadside and PEMS measurements under different lowest percentiles and time windows. Considering that the cutoff particle sizes of CPC and PEMS were inconsistent in this study, the effects of different time windows (1 and 5 min) and lowest percentiles (lowest 10 value average value, lowest 1, 5, 10, 20, and 30 percentiles) on NO emission factor estimation were evaluated by comparing the HEI and onboard PEMS measurement NO emission factors to evaluate the reliability and accuracy of this method. As shown in Figs. S4(a)–S4(f), the results demonstrate that the 10-percentiles and 20-percentiles in the 5-min time windows (Figs. S4(d) and S4(e)) have better performance (slope = 0.97, R^2 = 0.95) in the NO emission factors calculation than other time windows and lowest percentile settings (Figs. S4(a)–S4(c) and S4(f)). In addition, other time windows and lowest percentile settings presented significantly underestimated (points in the red circle in Fig. S4). Therefore, a 5-min time window and the lowest 10-percentile were selected to calculate the background concentrations in this study. The on-road vehicle emitted concentrations of ΔNO, ΔPN, and ΔCO_2 were obtained by subtracting the background value from the HEI measured concentrations.

Second, peaks in the on-road vehicle-emitted pollutant concentrations were detected. In this step, the selected peaks, namely peak 1, should follow several base criteria: 1) higher than neighboring values, 2) higher than the limit of detection (LOD), which is three times the standard deviation of the background signal, 3) the distance between two adjacent peaks is no less than 3 s, and 4) the CO_2 concentration is normally used to normalize the NO and PN concentrations to compensate for different degrees of dilution between

the vehicle exhaust emission and instrument measurement. In addition to the aforementioned base criteria, a threshold for the ΔCO_2 peaks was required to ensure the accuracy of the emission factor calculations. According to previous studies (Zhou et al., 2020; Xiang et al., 2023), this ΔCO_2 peak threshold was set as 5 ppm in this study.

To match the detected spikes to the passing vehicle exhaust plumes, a time alignment algorithm was proposed to determine whether detected vehicle-emitted concentration peaks (peak 1) were the responses of the passed vehicle exhaust plume. Because of the different instrument response times, when the test vehicles drove past the sensor platform, the appearance times of the NO, PN, and CO_2 peaks differed. Therefore, the appeared times of ΔNO, ΔPN, and ΔCO_2 peaks and time differences between CO_2 with NO ($\Delta t_{NO\_CO_2}$) and PN ($\Delta t_{PN\_CO_2}$) were determined according to field experiment measurement results. As shown in Fig. S5(a), these signal peaks typically appear within 1–10 s of the test vehicles passing through the sensor platform. In addition, most of the $\Delta t_{NO\_CO_2}$ and $\Delta t_{PN\_CO_2}$ values are gathered within the range of −5 to 5 s (Fig. S5(b)). If there is a ΔCO_2 peak within 5 s before or after the ΔPN or ΔNO peak, these peaks are considered as matched peaks (Fig. 2(a)). For unmatched peaks, if the ΔPN or ΔNO peak exceeds 10 times the deviation of the background signal, namely the limit of quantification (LOQ), these peaks were also selected for further vehicle exhaust plumes identification (Fig. 2(b)). This was done to avoid misjudgment owing to CO_2 concentrations below the thresholds mentioned above. The pollutant peaks that met the aforementioned standards were defined as peaks 2. If there were peaks 2 of ΔPN or ΔNO within 10 s after the vehicle past the HEI platform, these peaks 2 were believed to be the successfully captured plumes and this vehicle was namely successfully identified vehicles. If multiple vehicles pass through the observation station in close succession, they are identified as forming part of a fleet.

Fuel-based NO and PN emission factors of the successfully identified vehicle plumes were calculated using the carbon balance method (Shen et al., 2022; Xiang et al., 2023). Previous studies (Zhang et al., 2014; Preble et al., 2015) have indicated that the proportion of carbon in CO, BC, and HC is typically less than 2% of the total fuel carbon. The primary carbonaceous product resulting from the combustion of vehicle fuel is CO_2 (> 95% by mass) (Preble et al., 2015). The sensitivity of CO_2 to the emission factor calculation was several orders of magnitude higher than those of CO and BC (Preble et al., 2015). The exclusion of CO, BC, and HC had a negligible effect on the emission factors calculation. Consequently, the fuel-

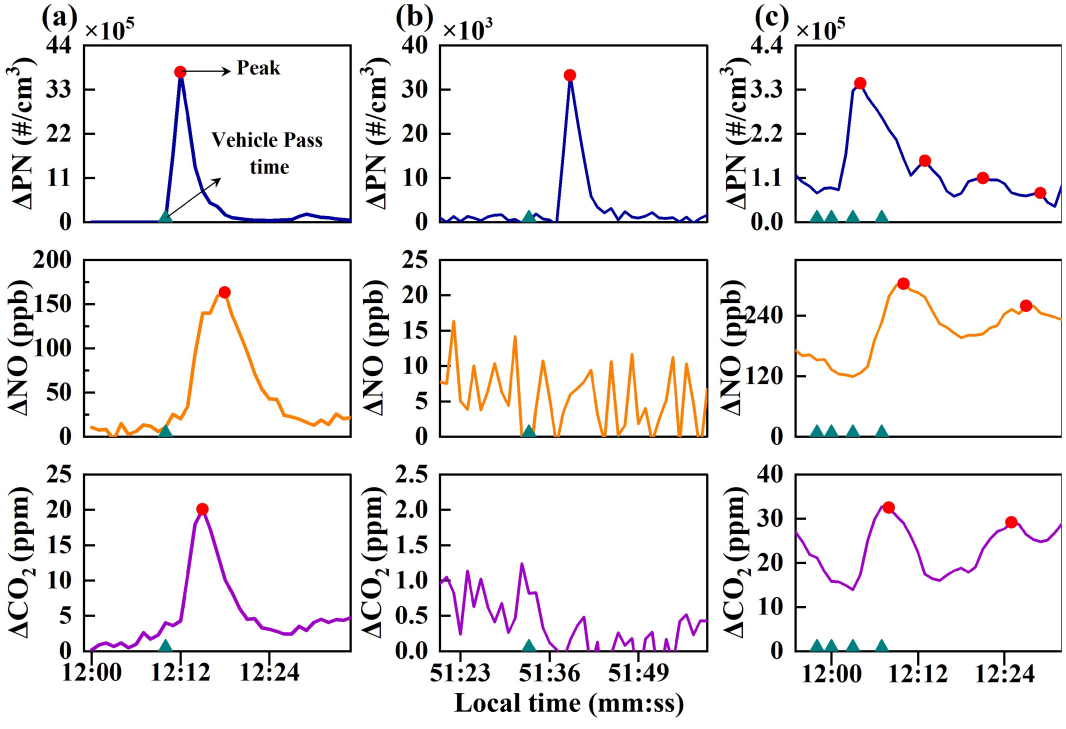

Fig. 2 Time series of pollutant signals during continuous drive-throughs (a) matched peaks, (b) unmatched peaks, and (c) fleet passed.

based emission factors of NO and PN were derived from the formula proposed by Wang et al. (2012), which assumes that all carbon in the fuel is converted to CO_2. The emission factors of NO and PN were calculated using the following Eq. (2). In addition, several methods can be used to compute fuel-based emission factors, such as the differential (Raparthi et al., 2023), integration (Raparthi et al., 2023), and peak height methods (Shen et al., 2022). The peak height method was selected in this study, with the peak height of vehicle-emitted pollutant concentrations being utilized for the calculation of emission factors, as opposed to integrating the peak area. This method is suitable for high traffic densities in real-world urban environment.

$$EF_{\mathrm{p}} = \frac{\Delta[\mathrm{P}]}{\Delta[\mathrm{CO_2}]} \times w_c, \quad (2)$$

where EF_{p} is the vehicle emission factor of the target pollutants NO and PN. $\Delta[\mathrm{P}]$ is the vehicle-contributed concentration peak height of ΔNO (ppb) and ΔPN (#/cm^3). $\Delta[\mathrm{CO_2}]$ is the vehicle contribution peak height of ΔCO_2 (ppm). w_c is the carbon fraction of fuel and was set to be 0.81 for the mixed fleet in this study (Raparthi et al., 2023).

Finally, if the fuel-based emission factors of NO (EF_{NO}) and PN (EF_{PN}) of the identified vehicle plume were higher than the high-emitter threshold, the vehicle was identified as a high emitter. In general, the outlier values of all identified vehicle EFs were set as high emitters in this study, and detailed information on the high emitter threshold settings can be found in Section 3.2. We conducted a blind test under real-world driving conditions at the Tangshan and Chengdu sites for different potential high-emitter thresholds to assess the uncertainty and effectiveness of the high-emitter thresholds for identifying high-emission vehicles. Furthermore, several high emitters were tested using PEMS (OBS-ONE, Horiba Ltd., Japan) with the assistance of traffic police officers (Tian et al., 2024) to validate the high emitter identification scheme. The emission factors for NO and PN by PEMS were calculated using the same carbon balance method, as previously described. The China VI emission standard was employed to determine whether the identified high emitters were in fact high emitters.

3 Results and discussion

3.1 Overview of measurement and vehicle identification

Figures 3 and S6 present a short section of second-by-second PN, NO, and CO_2 measured concentrations, background concentrations, identified vehicles, and corresponding emission factors at the Tangshan site (local time 2022-08-15 08:05–08:30) and Chengdu (local time 2023-04-06 08:05–08:30), respectively, as illustrative examples. Figure 4 shows the relative frequency histogram distributions and probability fitting curves for vehicle emission contributions, background values, and LOQ concentrations during the sampling period at the Tangshan and Chengdu sites. Generally, vehicular emission-contributed concentrations and LOQ show log-normal or highly skewed distributions. This is a common feature of on-road vehicle exhaust emission measurements (Zhou et al., 2020). In contrast, normal or weakly skewed distributions were observed for the background concentrations of NO, PN, and CO_2. NO and PN exhibited larger response signals to vehicle emissions. The vehicle emission-contributed concentrations of NO, PN, and CO_2 in Tangshan (Chengdu) were 32.9 ± 71.9 (27.7 ± 77.2) ppb, 8212.7 ± 59749.5 (5384.6 ± 46678.4) #/cm^3, and 7.3 ± 14.9 (8.2 ± 20.5) ppm, respectively. The average background concentrations of NO, PN, and CO_2 in Tangshan (Chengdu) were 347 ± 57.5 (481 ± 153) ppb, 14387 ± 11077 (9132 ± 5076) #/cm^3, and 442 ± 45.1 (426 ± 9.1) ppm, respectively. The vehicle-contributed pollutants concentration in Tangshan was higher than that in Chengdu, which might contribute to the relatively larger traffic density and a higher percentage of heavy-duty diesel trucks (16.3%, Fig. S2(a)) than that in Chengdu (5%, Fig. S2(b)). Previous studies have demonstrated that the PN emissions of heavy-duty vehicles are approximately 20 times higher than those of light-duty vehicles (Wang et al., 2012). Numerous cars may identify the same pollutant peak, namely, fleets (Fig. 2(c)). Figure 3 depicts multiple vehicles passing at 08:15 and approximately 30 s, with concentrations remaining high. The methodology employed in this study could not identify the high emitters within the fleet. However, subsequent analysis indicated that the exclusion of such high emitters had a negligible impact on the overall identification of high emitters.

According to the workflow scheme of high emitter identification via HEI measurement mentioned in Section 2.3, approximately 60% and 73% of vehicles that passed the HEI measurement sites were successfully detected, respectively (Fig. S7). A proportion of vehicle exhaust plumes was not detected, which may be attributed to the low emission levels of vehicles, diffusion, and dilution of vehicle exhaust plumes under adverse wind direction and speed conditions (Sahlodin et al., 2007). In addition, among

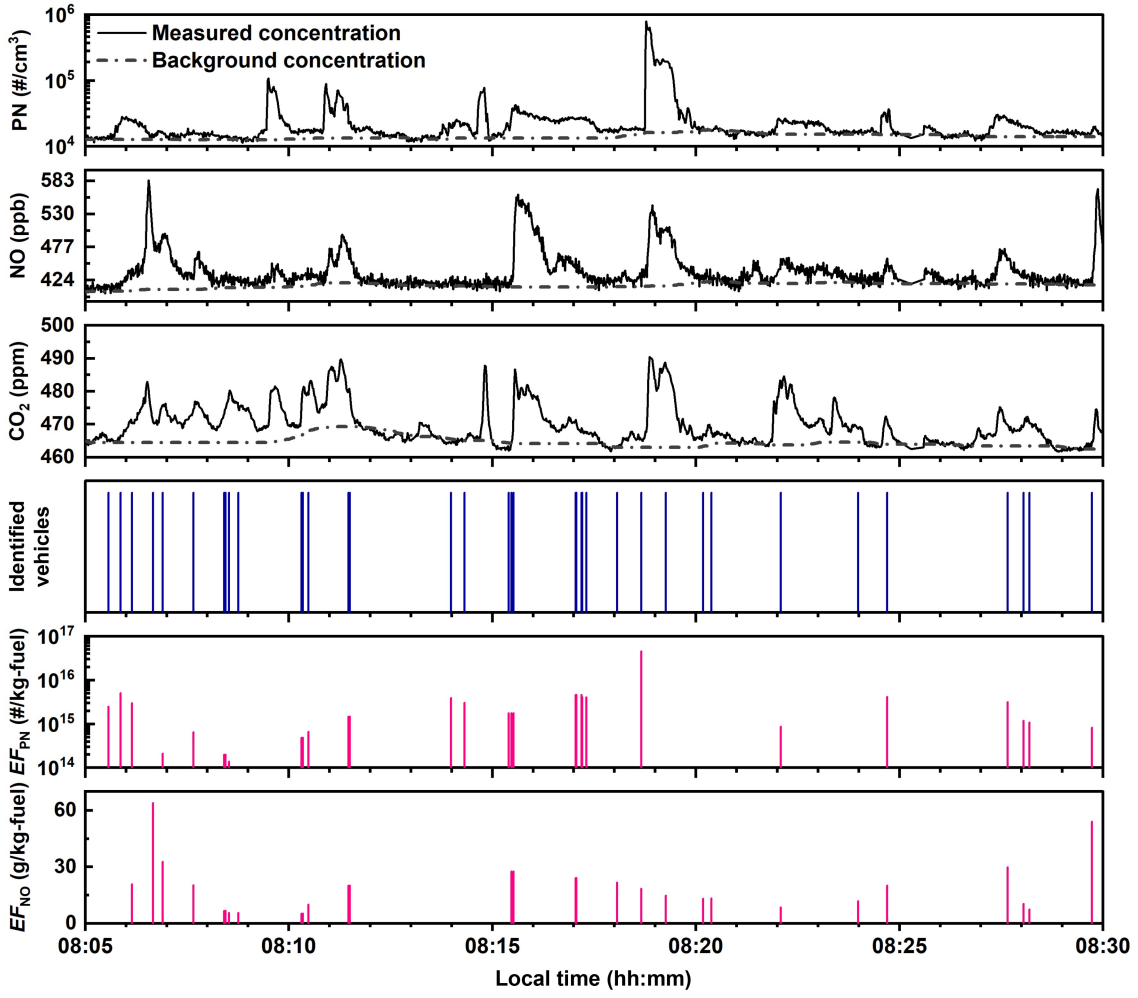

Fig. 3 Measured concentration, background concentration, and identified vehicle emission concentration peaks of PN, NO, and CO_2 at Tangshan from 8:05 to 8:30 a.m. on 16 August 2022.

the unidentified vehicles by roadside sensors at the Tangshan and Chengdu sites, only a few vehicles were identified as high-emitters (less than 2%) by RS sensors. Overall, a higher percentage of vehicles identified by roadside sensors implies a superior performance of the HEI platform. Among the vehicles identified by roadside measurements, more than 99000 NO plumes in Tangshan, 28000 NO plumes in Chengdu, 87000 PN plumes in Tangshan, and 18000 PN plumes in Chengdu were successfully identified.

3.2 The emission factor distribution and high-emitter thresholds

EFs for the corresponding vehicle exhaust plumes were calculated using the carbon balance method proposed in Section 2.3. Figure 5 shows the histograms of the measured NO and PN EFs for the identified vehicles and the corresponding fitting curves of the EF distributions at the Tangshan and Chengdu sites during the sampling periods. The large sample size ensured sufficient data points for investigating the emission factor distribution characteristics. The NO and PN EFs tended to have log-normal distributions, with coefficients of determination (R^2) of 0.93 ($p < 0.001$) and 0.95 ($p < 0.001$), respectively. The mean EFs for NO and PN are 28.3 ± 59.5 g/kg-fuel and $8.6 \times 10^{15} \pm 4.5 \times 10^{16}$ #/kg-fuel, respectively. By contrast, the median values of NO and PN EFs are 14.3 g/kg-fuel and 1.3×10^{15} #/kg-fuel, respectively. The EFs distributions of NO and PN were highly skewed, which was mainly attributed to the strong influence of a small portion of high emitters (Wang et al., 2023). To the best of our knowledge, a small fraction of vehicles with failed exhaust after-treatment systems or those driven under high-emission conditions, such as overweight and

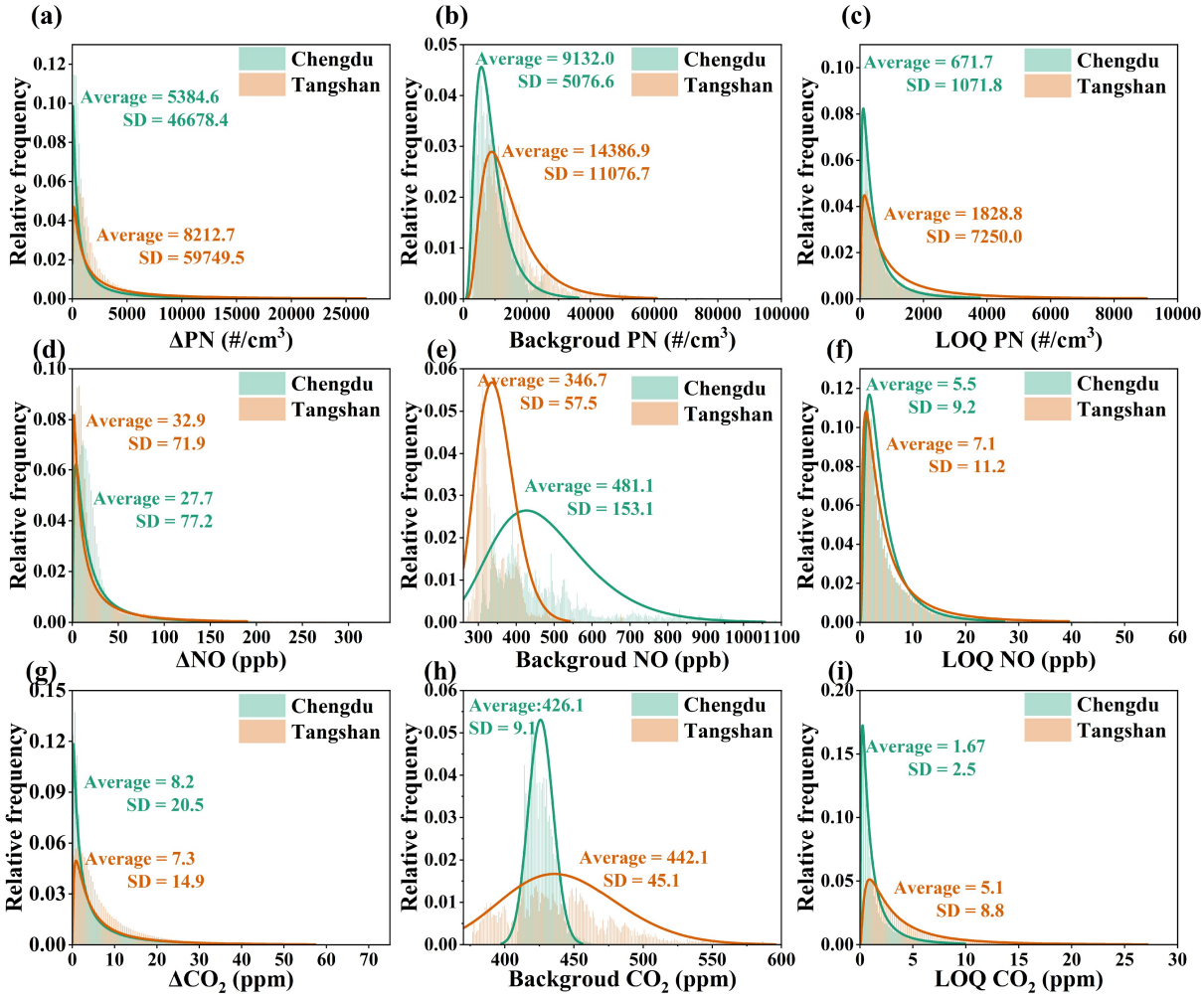

Fig. 4 Relative frequency distributions and fitting curves for the vehicle contributed concentrations (a, d, g), background values (b, e, h), and LOQ concentrations (c, f, i) of PN, NO, and CO_2 in the Tangshan and Chengdu sites.

severe traffic congestion, have the potential to emit pollutants that are several orders of magnitude higher than those emitted by well-maintained vehicles under normal driving conditions (Ježek et al., 2015).

In this study, the fraction of high emitters was determined using the box distribution method, and the outlier points whose *EF* values exceeded the third quartile plus 1.5 times the inter-quartile range (Q3 + 1.5IQR) were defined as high emitters. The box plot distributions of EF_{NO} and EF_{PN} for different vehicle and fuel types at Tangshan and Chengdu are shown in Fig. S8. The high emitter thresholds of the EF_{NO} for gasoline passengers (GPs), light gasoline trucks (LGTs), light diesel trucks (LDTs), and heavy diesel trucks (HDTs) are 65, 60, 59, and 58 g/kg-fuel, respectively. The high-emitter thresholds of EF_{PN} for gasoline passengers (GPs), light gasoline trucks (LGTs), light diesel trucks (LDTs), and heavy diesel trucks (HDTs) were 1.0×10^{16}, 1.1×10^{16}, 1.1×10^{16}, 9.5×10^{16} #/kg-fuel in this study, respectively. Considering that there were no significant differences in the high emitter thresholds for different vehicle and fuel types, the high emitter thresholds of EF_{NO} and EF_{PN} were defined using the box plot distribution of the total identified vehicles in this study. A box plot distribution of the total identified vehicle EFs for NO and PN is shown in Fig. 6. The high-emitter thresholds of EF_{NO} and EF_{PN} were 65 g/kg-fuel and 1.0×10^{16} #/kg-fuel in this study, which were 4.5 and 7.5 times higher than the median values of EF_{NO} and EF_{PN}. The high emitter thresholds of EF_{NO} and EF_{PN} were used in combination to identify the high-emitters. If either EF_{NO} or EF_{PN} was greater than the corresponding threshold, the vehicle was identified as a high emitter.

Higher emitter thresholds are key factors in the successful identification of high emitters. Therefore, we

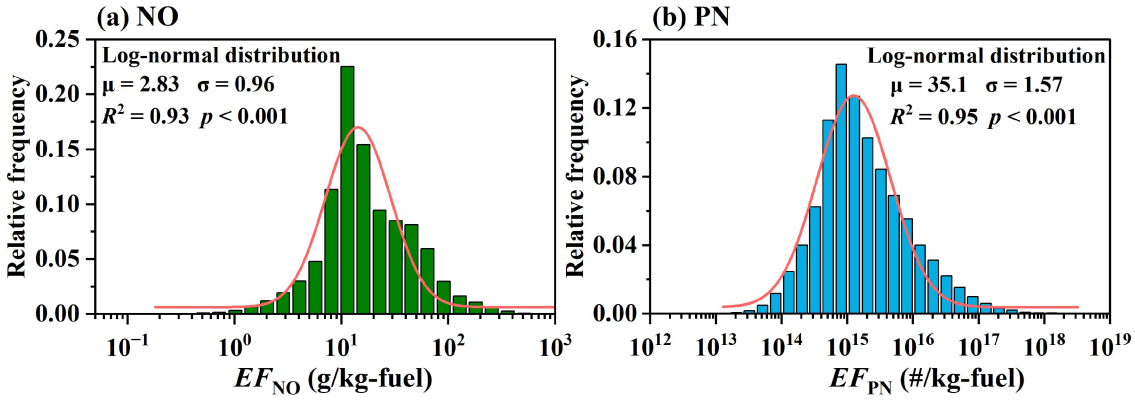

Fig. 5 Histograms of measured (a) NO and (b) PN EFs for total identified vehicles and corresponding fitting curves of the EF distributions.

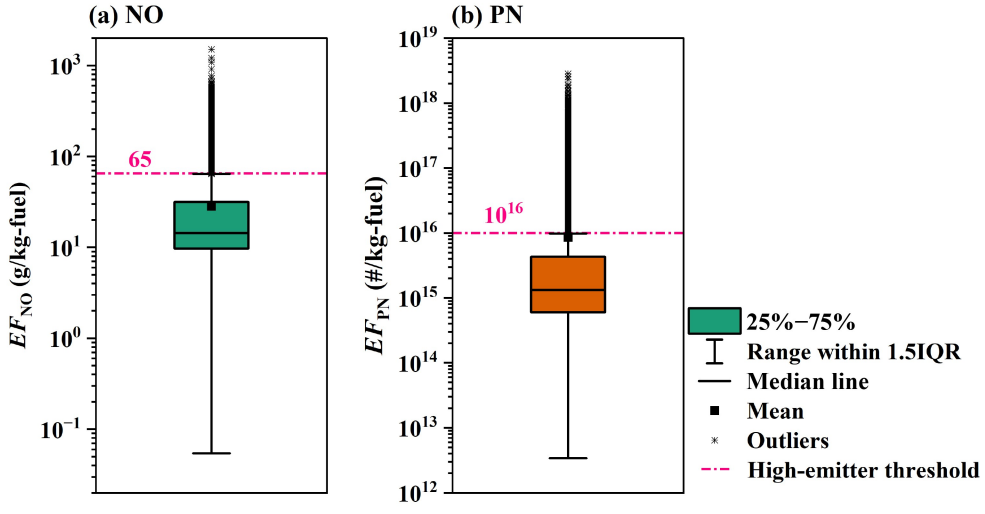

Fig. 6 Boxplot of (a) EF_{NO} and (b) EF_{PN} distribution. Note: The bottom and top whiskers out of the box represent the Q1–1.5 IQR and Q3 + 1.5 IQR, respectively. Outlier points are values larger than Q3 + 1.5 IQR, which are identified as high-emitters in this study.

conducted a blind test using 976 vehicles (including 727 high-emitting and 249 clean vehicles) to calculate the high-emitter false alarm rate (false-identified high-emitters/identified emitters) and high emitter miss rate (actual high-emitters classified as clean vehicles/actual high-emitters) under real-world driving conditions at the Tangshan and Chengdu sites for different potential high-emitter thresholds of EF_{NO} from 30 to 75 g/kg-fuel and EF_{PN} from 2×10^{15} to 2×10^{16} #/kg-fuel. From Fig. 7, it is evident that with an increase in EF_{NO} and EF_{PN} thresholds, the high-emitter false alarm rate decreased from 30% to 2%, and the high-emitter miss rate increased from 50% to 75%, respectively. This high miss rate can be attributed to the fact that high emitters can also have low instantaneous emissions. Both the false alarm and miss rates should be considered when setting high-emitter cut-off thresholds. Considering public trust in high-emitter identification results, a low false alarm rate might be appealing to policymakers, as it places a light burden on the drivers of clean vehicles (Qiu and Borken-Kleefeld, 2022). Therefore, the false alarm rate should be limited to a reasonable range, such as below 10% or 5%. When the high-emitter thresholds of EF_{NO} and EF_{PN} were set to be 60 g/kg-fuel and 1.1×10^{16} #/kg-fuel, the false alarm rate was below 5%, and relatively more high-emitters were successfully identified. The high-emitter cut-off thresholds of EF_{NO} and EF_{PN} determined at a false alarm rate of 5% level are very close to that by the box plot distribution method used in this study. When the high-emitter thresholds of EF_{NO} and EF_{PN} are set to be 65 g/kg-fuel and 1.0×10^{16} #/kg-fuel, approximately

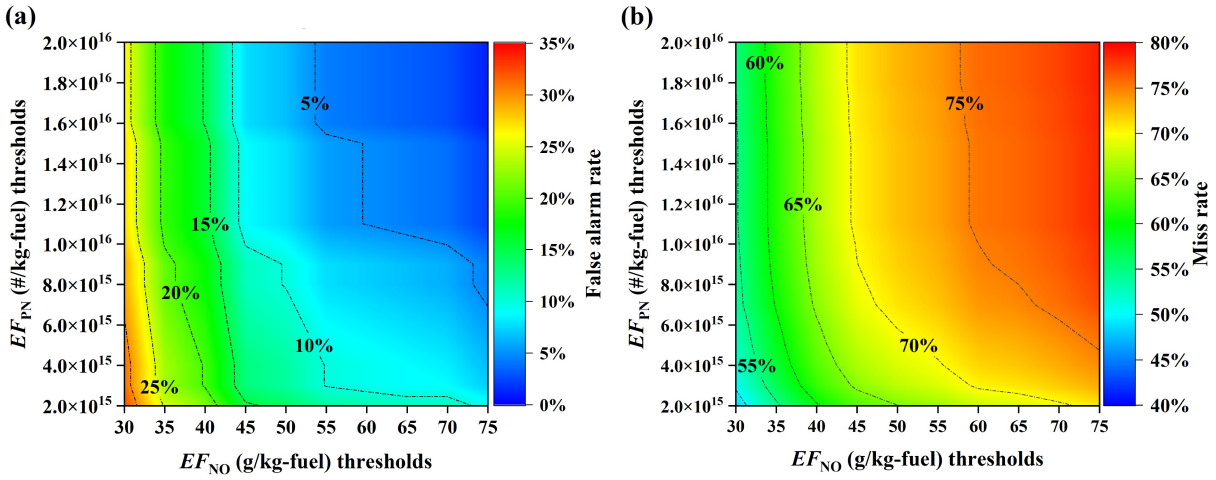

Fig. 7 The (a) blind test identification high-emitter false alarm rate (falsely identified high-emitters/identified-emitters) and (b) high-emitters miss rate (actual high-emitters classified as clean vehicles/actual high-emitters) under different high-emitter thresholds.

27% high-emitters can be identified at 5% false alarm rate level, which reflects that the high-emitter thresholds determined in this study are reasonable. Qiu and Borken-Kleefeld (2022) used 48 EU-5D passenger vehicles from the European Mobile Emission Sources Study (ERMES) database to perform 163 RS sensor measurements, and results demonstrated that only 29% of high-emitters were identified from the total high-emitters at a 75% precision level with one measurement. The roadside HEI and RS measurements have high miss rates of high emitters with a single measurement. More high emitters can be identified with repeated measurements at a low false alarm rate level (i.e., 5%), and the low cost of the roadside HEI platform makes it more suitable for mass application in real-world high emitters identification.

3.3 High-emitter and on-site inspection

In general, the percentage of high-emitters identified in individual vehicles at the Tangshan and Chengdu sites was 9.6% of the total identified vehicles (Fig. 8(a)). This result was similar to that from previous studies reported in India (14%) (Raparthi et al., 2023), USA (13%) (Park et al., 2016), China (20%–23%) (Wang et al., 2011; Huo et al., 2012), but was slightly higher than the high-emitter percentages identified using RS measurement at Tangshan and Chengdu sites in this study, with the values of 8.3% and 3.2%, respectively. Specifically, the high-emitter percentages of NO and PN that exceeded the high-emitter thresholds for individual vehicles at the Tangshan site were 4.1% and 5.4%, respectively (Fig. 9). The high-emitter percentages of NO and PN EFs exceeding the high-emitter thresholds at the Chengdu site were 10.6% and 2.6%, respectively. In addition, the contribution of high-emitter emissions to the total identified vehicular emissions was investigated. 5.4% NO and 4.1% PN high-emitters contributed approximately 30.9% NO and 75.7% PN to the total identified vehicle emissions at the Tangshan site. At Chengdu sites, 10.6% NO and 2.6% PN high-emitters contributed approximately 57.7% NO and 72.1% PN to the total identified individual vehicle emissions. These results demonstrate that on-road vehicle emissions can be effectively reduced by maintaining post-treatment devices and replacing older vehicles (Ježek et al., 2015).

Furthermore, a proportion vehicles were categorized as fleets. As shown in Fig. 9, among the identified vehicles, approximately 26% and 24% were identified as fleets at the Tangshan and Chengdu sites, respectively. High emitters in the fleets accounted for approximately 4% and 4.6% of all identified vehicles at the Tangshan and Chengdu sites, respectively. Notably, it is difficult to identify an actual single high emitter from a fleet using the current algorithm. This may result in the inadvertent classification of some normal vehicles as high-emitters. As shown in Fig. S9, there was no significant difference in the identified high emitter percentages at the Tangshan and Chengdu sites between the fleets and the excluding fleets. These results indicate that the exclusion of high emitters from the fleet had a negligible impact on the overall identification results of high emitters. Thus, it follows that high emitters in the fleet are classified as suspected high emitters and undergo further testing.

Moreover, the ideal method for validating the high-emitter identification scheme is to conduct confirmatory

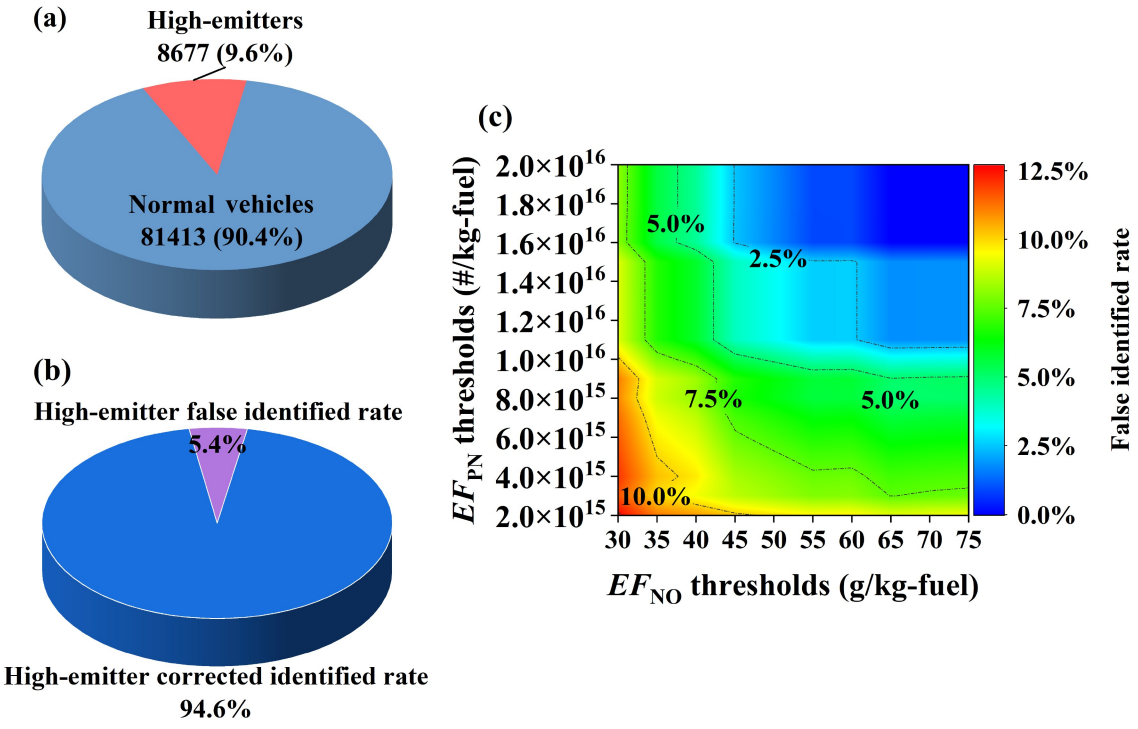

Fig. 8 (a) High-emitter percentage of real-world identification, (b) on-site inspection of identified high-emitters, (c) on-site high-emitter false identified rate of varying thresholds.

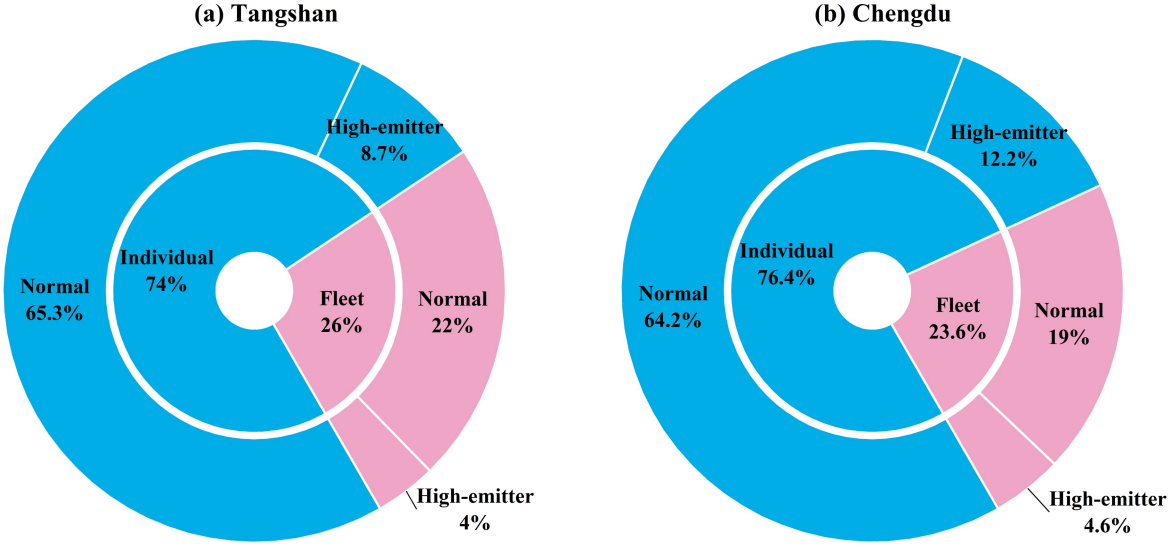

Fig. 9 High-emitter percentages of individual and fleet vehicles at (a) Tangshan and (b) Chengdu sites.

testing of these vehicles using PEMS/chassis tests (Qiu and Borken-Kleefeld, 2022). In this study, we tested a few identified high emitters by conducting on-site inspections of vehicle exhaust after-treatment systems and performing PEMS testing with the assistance of the traffic police. Overall, 122 identified high-emitters were inspected, and the false alarm rate was 5.4% (Fig. 8(b)). If the high-emitter thresholds of NO and PN increase to 70 g/kg-fuel and 1.6×10^{16} #/kg-fuel, respectively, the on-site inspection high-emitter false alarm rate can be closed to zero (Fig. 8(c)). Relatively lower false-alarm rates of the on-site inspections demonstrating that our algorithm performs well in identifying real-world high emitters.

4 Conclusions and implications

Real-world high-emitter identification plays an important role in controlling vehicular emission pollutants. In this study, a low-cost roadside HEI platform was used for online roadside measurements of vehicle-emitted NO, PN, and CO_2 concentrations. Based on more than one month of HEI measurement data sets, a novel comprehensive scheme was developed for real-world high-emissions identification. Slightly larger high-emitter percentages of the roadside HEI platform (9.6%) than RS measurement (3.2%–8.3%) were found in this study. The roadside HEI platform identified high-emitters contributed 30.9%–57.7% NO and 72.1%–75.5% PN emission of the total identified individual vehicles.

High-emitter thresholds have a significant impact on the high-emitter identification false-alarm and miss rates. A low false alarm rate implies a high miss rate for the detection of high emission vehicles. Therefore, we suggest a low false alarm rate (below 5%) might be appealing to policymakers, as it places a light burden on drivers of clean vehicles. Moreover, with a single instantaneous measurement, the roadside HEI platform and RS sensor showed larger high-emitter miss rate. With repeated measurements, improvements in high-emitter identification were even more significant. The advantages of low cost and convenient mobility make roadside HEI platforms suitable for large-scale applications in real-world high-emitter identification. Furthermore, although 65 g/kg-fuel for NO and 10^{16} #/kg-fuel for PN were suggested in this study, the high emission thresholds of EF_{NO} and EF_{PN} can be determined based on the requirements of local regulatory authorities.

Finally, there are some limitations to and suggestions for the roadside HEI platform measurement approach. First, a large number of vehicles that passed the HEI platform were not detected, most probably because of changes in wind direction, leading to the plume not reaching the roadside platform to be detected. Therefore, HEI platforms should be placed on both sides of the road to increase the chances of detecting emission plumes under various wind conditions. Second, the roadside sensors and RS measurements showed a larger miss rate and uncertainty for high emitters, with a single instantaneous measurement. Therefore, the joint application of these two methods can enhance the measurement of gaseous and particulate pollutants and reduce the uncertainty and miss rate of high-emitter identification. If the vehicle is frequently listed as a suspected high emitter over a certain period of time, such as more than three times a month, it will be identified as a high emitter and will receive a citation for further inspection. Overall, the roadside HEI platform developed in this study represents a promising approach for real-world high-emitter identification. Its low cost, mobility, and strong adaptability significantly enhance the network-monitoring capability of urban supervision departments and directly promote the coordinated management of road traffic and air quality.

Conflict of Interests The authors declare that they have no known competing financial interests or personal relationships that could have appeared to influence the work reported in this paper.

Acknowledgements We acknowledge support from the National Key R&D Program of China (No. 2023YFC370540203) and the China Postdoctoral Fellowship Program of CPSF (No. GZC20231271).

Electronic Supplementary Material Supplementary material is available in the online version of this article at https://doi.org/10.1007/s11783-025-1983-x and is accessible for authorized users.

References

Anenberg S C, Miller J, Minjares R, Du L, Henze D K, Lacey F, Malley C S, Emberson L, Franco V, Klimont Z, et al. (2017). Impacts and mitigation of excess diesel-related NO_x emissions in 11 major vehicle markets. Nature, 545(7655): 467–471

Apte J S, Messier K P, Gani S, Brauer M, Kirchstetter T W, Lunden M M, Marshall J D, Portier C J, Vermeulen R C H, Hamburg S P (2017). High-resolution air pollution mapping with google street view cars: exploiting big data. Environmental Science & Technology, 51(12): 6999–7008

Arvind T, Marc C B, Pragalath T, Saroj P, Daniel C, Hemanth K, Mridul G, Adewale O, Henry H, Matt M (2015). Emission rates of regulated pollutants from current technology heavy-duty diesel and natural gas goods movement vehicles. Environmental Science & Technology, 49(8): 5236–5244

Bancă G, Ivan F, Toma M, Nişulescu V, Micu D A (2024). Experimental research on vehicles equipped with a GMP hybrid for the new Euro 7 emissions standard. IOP Conference Series. Materials Science and Engineering, 1303(1): 012026

Bishop G A, Haugen M J, Mcdonald B C, Boies A M (2022). Utah wintertime measurements of heavy-duty vehicle nitrogen oxide emission factors. Environmental Science & Technology, 56(3): 1885–1893

Bishop J D K, Molden N, Boies A M (2019). Using portable emissions measurement systems (PEMS) to derive more accurate estimates of fuel use and nitrogen oxides emissions from modern Euro 6 passenger cars under real-world driving conditions. Applied Energy, 242: 942–973

Blanco M N, Bi J, Austin E, Larson T V, Marshall J D, Sheppard L

(2023). Impact of mobile monitoring network design on air pollution exposure assessment models. Environmental Science & Technology, 57(1): 440–450

Bousiotis D, Allison G, Beddows D C S, Harrison R M, Pope F D (2023). Towards comprehensive air quality management using low-cost sensors for pollution source apportionment. npj Climate and Atmospheric Science, 6(1): 1–10

Boveroux F, Cassiers S, Buekenhoudt P, Chavatte L, De Meyer P, Jeanmart H, Verhelst S, Contino F (2019). Feasibility Study of a New Test Procedure to Identify High Emitters of Particulate Matter During Periodic Technical Inspection. SAE Technical Paper, 2019-01-1190. Warrendale: SAE International

Camilleri S F, Montgomery A, Visa M A, Schnell J L, Adelman Z E, Janssen M, Grubert E A, Anenberg S C, Horton D E (2023). Air quality, health and equity implications of electrifying heavy-duty vehicles. Nature Sustainability, 6(12): 1643–1653

Carter S A, Rahman M M, Lin J C, Shu Y H, Chow T, Yu X, Martinez M P, Eckel S P, Chen J C, Chen Z, et al. (2022). In utero exposure to near-roadway air pollution and autism spectrum disorder in children. Environment International, 158: 106898

Chen X, Jiang L, Xia Y, Wang L, Ye J, Hou T, Zhang Y, Li M, Li Z, Song Z, et al. (2022). Quantifying on-road vehicle emissions during traffic congestion using updated emission factors of light-duty gasoline vehicles and real-world traffic monitoring big data. Science of the Total Environment, 847: 157581

Chu M, Brimblecombe P, Wei P, Liu C H, Du X, Sun Y, Yam Y S, Ning Z (2022). Kerbside NO_x and CO concentrations and emission factors of vehicles on a busy road. Atmospheric Environment, 271: 118878

Deng F, Lv Z, Qi L, Wang X, Shi M, Liu H (2020). A big data approach to improving the vehicle emission inventory in China. Nature Communications, 11(1): 2801

Feng R, Hu X, Li G, Sun Z, Deng B (2022). A comparative investigation between particle oxidation catalyst (POC) and diesel particulate filter (DPF) coupling aftertreatment system on emission reduction of a non-road diesel engine. Ecotoxicology and Environmental Safety, 238: 113576

Ghaffarpasand O, Ropkins K, Beddows D C S, Pope F D (2023). Detecting high emitting vehicle subsets using emission remote sensing systems. Science of the Total Environment, 858: 159814

Heerah S, Frausto-Vicencio I, Jeong S, Marklein A R, Ding Y, Meyer A G, Parker H A, Fischer M L, Franklin J E, Hopkins F M, et al. (2021). Dairy methane emissions in California's san Joaquin valley inferred with ground-based remote sensing observations in the summer and winter. Journal of Geophysical Research-Atmospheres, 126(24): e2021JD034785

Hilker N, Wang J M, Jeong C H, Healy R M, Sofowote U, Debosz J, Su Y, Noble M, Munoz A, Doerksen G, et al. (2019). Traffic-related air pollution near roadways: discerning local impacts from background. Atmospheric Measurement Techniques, 12(10): 5247–5261

Hu Z, Lu Z, Song B, Quan Y (2021). Impact of test cycle on mass, number and particle size distribution of particulates emitted from gasoline direct injection vehicles. Science of the Total Environment, 762: 143128

Huang Y, Lee C K C, Yam Y S, Mok W C, Zhou J L, Zhuang Y, Surawski N C, Organ B, Chan E F C (2022). Rapid detection of high-emitting vehicles by on-road remote sensing technology improves urban air quality. Science Advances, 8(5): eabl7575

Huang Y, Organ B, Zhou J L, Surawski N C, Hong G, Chan E F C, Yam Y S (2018). Emission measurement of diesel vehicles in Hong Kong through on-road remote sensing: performance review and identification of high-emitters. Environmental Pollution, 237: 133–142

Huang Y, Yu Y, Yam Y S, Zhou J L, Lei C, Organ B, Zhuang Y, Mok W C, Chan E F C (2020). Statistical evaluation of on-road vehicle emissions measurement using a dual remote sensing technique. Environmental Pollution, 267: 115456

Huo H, Yao Z, Zhang Y, Shen X, Zhang Q, He K (2012). On-board measurements of emissions from diesel trucks in five cities in China. Atmospheric Environment, 54: 159–167

Ježek I, Katrasnik T, Westerdahl D, Mocnik G (2015). Black carbon, particle number concentration and nitrogen oxide emission factors of random in-use vehicles measured with the on-road chasing method. Atmospheric Chemistry and Physics, 15(19): 11011–11026

Kwon S, Park Y, Park J, Kim J, Choi K H, Cha J S (2017). Characteristics of on-road NO_x emissions from Euro 6 light-duty diesel vehicles using a portable emissions measurement system. Science of the Total Environment, 576: 70–77

Lei Y, Qin C, Qiu T, Yue G, Ding M (2021). NO_x emission removal from a parallel diesel engine group by scr system based on distributed control technology. Environmental Science & Technology, 55(9): 6352–6362

Lelieveld J, Evans J S, Fnais M, Giannadaki D, Pozzer A (2015). The contribution of outdoor air pollution sources to premature mortality on a global scale. Nature, 525(7569): 367–371

Li Y, Chen X, Wu J, Zhang Q, Zhang Z, Hao J, Jiang J (2024). A convertible condensation particle counter using alcohol or water as the working fluid. Aerosol Science and Technology, 59(2): 185–194

Liu B, Zimmerman N (2021). Fleet-based vehicle emission factors using low-cost sensors: case study in parking garages. Transportation Research Part D, Transport and Environment, 91: 102635

Liu H, He K, Lents J M, Wang Q, Tolvett S (2009). Characteristics of diesel truck emission in china based on portable emissions measurement systems. Environmental Science & Technology, 43(24): 9507–9511

Liu Q, Hallquist Å M, Fallgren H, Jerksjö M, Jutterström S, Salberg H, Hallquist M, Le Breton M, Pei X, Pathak R K, et al. (2019). Roadside assessment of a modern city bus fleet: gaseous and particle emissions. Atmospheric Environment: X, 3: 100044

Liu X, Elgowainy A, Vijayagopal R, Wang M (2021). Well-to-wheels analysis of zero-emission plug-in battery electric vehicle technology for medium- and heavy-duty trucks. Environmental

Science & Technology, 55(1): 538–546

Olin M, Oikarinen H, Marjanen P, Mikkonen S, Karjalainen P (2023). High particle number emissions determined with robust regression plume analysis (RRPA) from hundreds of vehicle chases. Environmental Science & Technology, 57(24): 8911–8920

Park S S, Vijayan A, Mara S L, Herner J D (2016). Investigating the real-world emission characteristics of light-duty gasoline vehicles and their relationship to local socioeconomic conditions in three communities in Los Angeles, California. Journal of the Air & Waste Management Association, 66(10): 1031–1044

Preble C V, Dallmann T R, Kreisberg N M, Hering S V, Harley R A, Kirchstetter T W (2015). Effects of particle filters and selective catalytic reduction on heavy-duty diesel drayage truck emissions at the port of Oakland. Environmental Science & Technology, 49(14): 8864–8871

Qiao X, Zhang Q, Wang D, Hao J, Jiang J (2021). Improving data reliability: a quality control practice for low-cost $PM_{2.5}$ sensor network. Science of the Total Environment, 779: 146381

Qiu M, Borken-Kleefeld J (2022). Using snapshot measurements to identify high-emitting vehicles. Environmental Research Letters, 17(4): 044045

Raparthi N, Barudgar A, Chu M, Ning Z, Phuleria H C (2023). Estimating individual vehicle emission factors from near-road measurements in India. Atmospheric Environment, 308: 119869

Raparthi N, Phuleria H C (2021). Real-world vehicular emissions in the Indian megacity: carbonaceous, metal and morphological characterization, and the emission factors. Urban Climate, 39: 100955

Raparthi N, Phuleria H C (2022). On-road vehicular emission characterization from the road-tunnel measurements in India: morphology, emission factors, and sources. Environmental Research, 215: 114295

Russell H S, Kappelt N, Fessa D, Frederickson L B, Bagkis E, Apostolidis P, Karatzas K, Schmidt J A, Hertel O, Johnson M S (2022). Particulate air pollution in the Copenhagen metro Part 2: Low-cost sensors and micro-environment classification. Environment International, 170: 107645

Sahlodin A M, Sotudeh-Gharebagh R, Zhu Y (2007). Modeling of dispersion near roadways based on the vehicle-induced turbulence concept. Atmospheric Environment, 41(1): 92–102

Shen Y, Zhang Q, Wang D, Tian M, Yu Q, Wang J, Yin H, Zhang S, Hao J, Jiang J (2022). Evaluation of a cost-effective roadside sensor platform for identifying high emitters. Science of the Total Environment, 816: 151609

Su CW, Yuan X, Shao XF, Moldovan N C (2023). Explore the environmental benefits of new energy vehicles: evidence from China. Annals of Operations Research,

Tian M, He L, Peng D, Fu M, Ma S, Mu J, Yu Q, Wang J, Yin H, Wang J (2024). Characterizing NO_x emissions from diesel trucks with tampered aftertreatment systems and its implications for identifying high emitters. Science of the Total Environment, 917: 170378

Tong Z, Li Y, Lin Q, Wang H, Zhang S, Wu Y, Zhang K M (2022). Uncertainty investigation of plume-chasing method for measuring on-road NO_x emission factors of heavy-duty diesel vehicles. Journal of Hazardous Materials, 424: 127372

Wang F, Fang D, Ketzel M (2012). Particulate number emission factors and charactization from road traffic. Acta Scientiarum Naturalium Universitatis Pekinensis, 48: 1023–1029

Wang H, Zhang S, Wu X, Wen Y, Li Z, Wu Y (2023). Emission measurements on a large sample of heavy-duty diesel trucks in china by using mobile plume chasing. Environmental Science & Technology, 57(40): 15153–15161

Wang J M, Jeong C H, Hilker N, Shairsingh K K, Healy R M, Sofowote U, Debosz J, Su Y, Mcgaughey M, Doerksen G, et al. (2018). Near-road air pollutant measurements: accounting for inter-site variability using emission factors. Environmental Science & Technology, 52(16): 9495–9504

Wang J M, Jeong C H, Zimmerman N, Healy R M, Hilker N, Evans G J (2017). Real-world emission of particles from vehicles: volatility and the effects of ambient temperature. Environmental Science & Technology, 51(7): 4081–4090

Wang J M, Jeong C H, Zimmerman N, Healy R M, Wang D K, Ke F, Evans G J (2015). Plume-based analysis of vehicle fleet air pollutant emissions and the contribution from high emitters. Atmospheric Measurement Techniques, 8(8): 3263–3275

Wang X, Westerdahl D, Wu Y, Pan X, Zhang K M (2011). On-road emission factor distributions of individual diesel vehicles in and around Beijing, China. Atmospheric Environment, 45(2): 503–513

Wei P, Brimblecombe P, Yang F, Anand A, Xing Y, Sun L, Sun Y, Chu M, Ning Z (2021). Determination of local traffic emission and non-local background source contribution to on-road air pollution using fixed-route mobile air sensor network. Environmental Pollution, 290: 118055

Wen Y, Wang H, Larson T, Kelp M, Zhang S, Wu Y, Marshall J D (2019). On-highway vehicle emission factors, and spatial patterns, based on mobile monitoring and absolute principal component score. Science of the Total Environment, 676: 242–251

Xiang S, Zhang S, Yu Y T, Wang H, Shen Y, Zhang Q, Wang Z, Wang D, Tian M, Wang J, et al. (2023). Evaluation of the relationship between meteorological variables and NO_x emission factors based on plume-chasing measurements. ACS ES&T Engineering, 3(3): 417–426

Yang Z, Tate J E, Rushton C E, Morganti E, Shepherd S P (2022). Detecting candidate high NO_x emitting light commercial vehicles using vehicle emission remote sensing. Science of the Total Environment, 823: 153699

Zeng L, Wang F, Xiao S, Zheng X, Li X, Xie Q, Yu X, Huang C, Hu Q, You Y, et al. (2024). Characterization and prediction of tailpipe ammonia emissions from in-use China 5/6 light-duty gasoline vehicles. Frontiers of Environmental Science & Engineering, 18(1): 6

Zhang S, Wu Y, Liu H, Huang R, Yang L, Li Z, Fu L, Hao J (2014).

Real-world fuel consumption and CO_2 emissions of urban public buses in Beijing. Applied Energy, 113: 1645–1655

Zheng Z, Durbin T D, Xue J, Johnson K C, Li Y, Hu S, Huai T, Ayala A, Kittelson D B, Jung H S (2014). Correction to comparison of particle mass and solid particle number (SPN) emissions from a heavy-duty diesel vehicle under on-road driving conditions and a standard testing cycle. Environmental Science & Technology, 48(3): 1779–1786

Zhou L, Hallquist Å M, Hallquist M, Salvador C M, Gaita S M, Sjödin Å, Jerksjö M, Salberg H, Wängberg I, Mellqvist J, et al. (2020). A transition of atmospheric emissions of particles and gases from on-road heavy-duty trucks. Atmospheric Chemistry and Physics, 20(3): 1701–1722